

Experimental Investigation of Single Expansion Ramp Nozzle (SERN) Flows with 20° Ramp Angle and 1h Cowl

Prasanth Samyakkannu^{1*}, Sam Daniel Fenny A², Yokesvaran K¹, Anand C¹

¹Assistant Professor, Department of Aerospace Engineering, Agni College of Technology, Chennai, India – 600 130

²Assistant Professor, Department of Mechanical Engineering, Agni College of Technology, Chennai, India – 600 130

Abstract. This experimental study investigates the velocity decay characteristics and mixing performance of a Single Expansion Ramp Nozzle (SERN) operating at low supersonic speeds. A SERN model with a 20° ramp angle and a one-hour cowl was created and tested over a range of low Nozzle Pressure Ratios (NPRs) of 3 to 6. The primary goal was to map the entire pressure field and measure the rapid loss of kinetic energy (velocity decay) downstream from the nozzle exit. A Pitot tube with a three-dimensional traverse mechanism was utilized to collect total pressure data along mutually perpendicular transverse axes at various axial locations (X/h and z/h). To ensure accuracy, a high-precision pressure scanner and indicator were utilized. Important data for assessing the SERN's performance at improving jet-ambient fluid mixing. The findings provide knowledge needed to adjust SERN geometry for increased propulsion efficiency.

1 Introduction

The use of Single Expansion Ramp Nozzles (SERNs) is also under consideration which has possible benefits in combined propulsion-airframe systems, where nozzle shape can have a significant impact on thrust and efficiency as well as vehicle performance[1]. The experimental results of the translation of the throating SERNs have also shown that the asymmetric ramp construction yields to alternative internal shock patterns and separation behavior, which do not occur in the case of axisymmetric nozzles [3]. The communications between expansion waves and external flow field are much influenced on the jet plume and surface pressure distribution along the ramp wall as in early computer representations. The shock-parted flow that occurs due to over-expanded working conditions is extremely susceptible to both geometric and operating parameters. Proper characterization is important in performance assessment [2]. Contemporary design studies have determined that the angle of the ramp, expansion ratio and cowl shape are significant factors in defining potential efficiency over a broad range of NPRs[6]. Plug-type and ramp-type propulsion system experiments have demonstrated that non-axisymmetric expansion devices have packaging benefits and structural simplicity, which can be useful in future launch vehicles [5].

* Corresponding author: prasanthaeb36@gmail.com

Based on the research on the nozzle selection criteria, asymmetric nozzles enhance those of the vectoring and minimizing the weight of a system [7]. With the investigations on side-expanding asymmetric nozzles, it turned out that the lateral expansion forms three dimensional structures in vertical direction, which influence the jet spreading and mixing behaviour to a great extent [14]. Hypersonic vehicle nozzles Airframe integrated nozzles were studied by optimization, which reported that ramp based designs are able to enhance pressure recovery, and minimise external drag [12]. Most recent work has discovered that the major factors that affect separation in large-expansion-ratio SERNs are both the behaviour of the boundary-layers and shock strength [13]. Experiments over-expanded wall jets at high speed which showed how the attachment, separation and re-attachment regions vary with varying ramp geometry provided useful analogies to the development of SERN jets [15]. A change in the geometry of ramps can have a strong influence on both shock-cell spacing and performance in plume decline as well as downstream mixing as demonstrated in literature [20].

2 Experimental Setup

The pressure readings were recorded by the use of a 16 channel PSI Model 9116 pressure transducer coupled to a Core i7 computer with the NUSS data acquisition software. Figure 3.6 depicts transducer employed in the experiments. The Model 9116 is capable of measuring pressures to 300 psi (approximately 20 atm) as well as giving a 1.5% error of full scale allowing it to re-zero the instrument after a re-zero calibration. To guarantee quality readings, the re-zero operation was conducted prior to each test run so that any offset errors may be removed. With this software interface, all the necessary functions were executed at ease and with ease, such as, initiation, reset, re-zero calibration and pressure-reading. The experimental apparatus consists of a compressed-air supply, flow-conditioning apparatus, and measurement system with which the jet out of the settling chamber was investigated. The air generated by a three-compressor unit is stored in three reservoir tanks so that there is a constant supply, and then is passed through a control valve and conditioning unit that has a moisture separator and pressure controller to stabilize the inlet pressure. The conditioned air is introduced into the settling chamber after additional adjustment, disturbances to flow are eliminated and it escapes via the nozzle well-defined and clean.

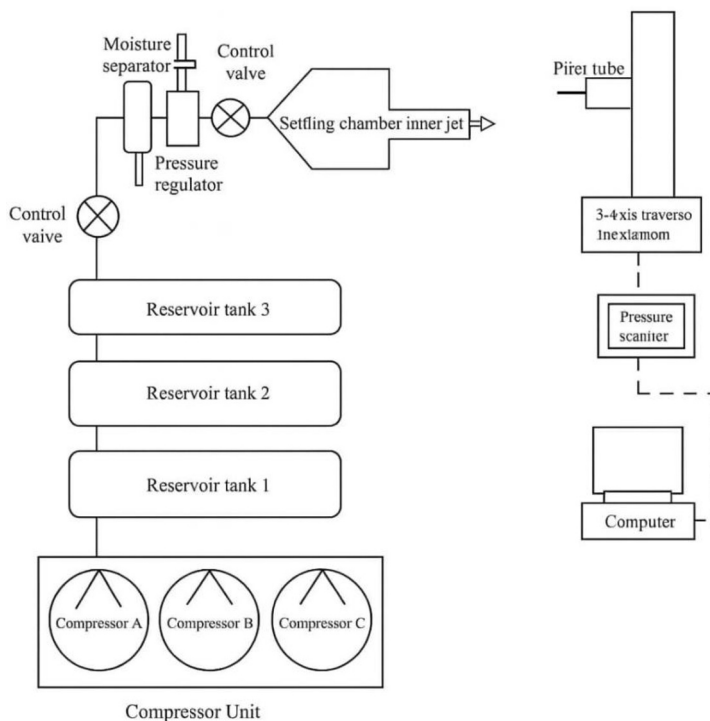


Fig. 1. Schematic diagram of jet facility

The jet properties are monitored by placing a Pitot tube on a 3 axis traverse mechanism, which allows precise spatial location and mapping of velocity distributions. The data of pitot pressure are sent to a pressure scanner where they are recorded and processed by a computer-based system of data acquisition. This design permits regulated flow provision and accurate quantification of jet characteristics that is important in aerodynamic studies.



Fig.2. Supersonic free jet facility at MIT

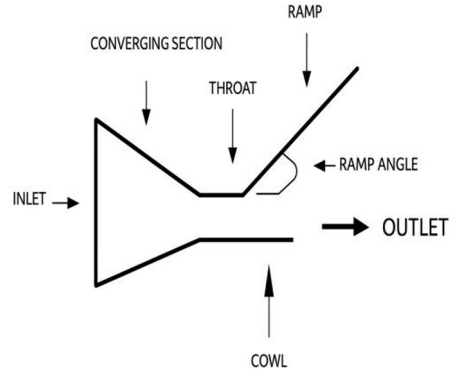


Fig. 3. Schematic Representation of SERN



Fig. 4. Model 9116 Intelligent Pressure scanner

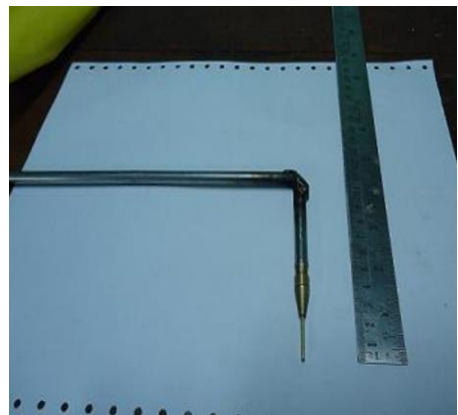


Fig. 5. Photographic view of Pitot tube

2.1 Experimental Procedure

The Single Expansion Ramp Nozzle (SERN) used in this study (Figure 2) consists of a converging nozzle, a 20° upper ramp, and a 1h cowl, all fabricated from stainless steel to withstand high temperatures and maintain structural rigidity. Experiments were conducted over nozzle pressure ratios (NPRs) ranging from 3 to 6 to examine how the jet behaves under different levels of expansion. For each NPR setting, the pressure-regulating valve connected to the settling chamber was carefully adjusted to achieve the required stagnation pressure, ensuring that the upstream flow remained steady and uniform throughout the tests.

To capture jet characteristics, a metallic Pitot tube mounted on a three-dimensional traverse system was employed, allowing precise measurements of total pressure at various positions within the jet plume along three mutually perpendicular axes. These measurements provide detailed insight into the jet's spatial development, shock structure, and expansion behaviour. From the collected pressure data, non-dimensional velocity profiles in the Y and Z directions were generated to study lateral and vertical jet spread, as well as any asymmetry induced by the SERN geometry.

The Pitot probe was connected to a high-accuracy pressure sensor interfaced with a computer for continuous data acquisition. Prior to testing, the pressure sensor and indicator were calibrated using a mercury manometer to ensure that measurement errors remained within acceptable limits.

The Mach number at each point, denoted as M_1 , was determined using the measured Pitot pressure P_0 . For subsonic regions, Equation (1) was applied because the Pitot pressure directly corresponds to the stagnation pressure of the flow. In contrast, in supersonic regions, a normal shock forms ahead of the Pitot probe, and therefore Equation (2) was used to account for compressible-flow effects and the post-shock stagnation pressure. The static pressure throughout the jet field is represented by P_1 . Since the jet discharges into still ambient air, pressure variations outside the core region were assumed to be negligible [5].

$$\frac{P_0}{P_1} = \left[1 + \frac{\gamma-1}{2} M_1^2 \right]^{\frac{\gamma}{\gamma-1}} \quad (1)$$

$$\frac{P_0}{P_1} = \left[\frac{(\gamma+1)M_1^2}{(\gamma-1)M_1^2+2} \right]^{\frac{\gamma}{\gamma-1}} \left[\frac{\gamma+1}{2\gamma M_1^2 - (\gamma-1)} \right]^{\frac{1}{\gamma-1}} \quad (2)$$

3 Results and Discussion

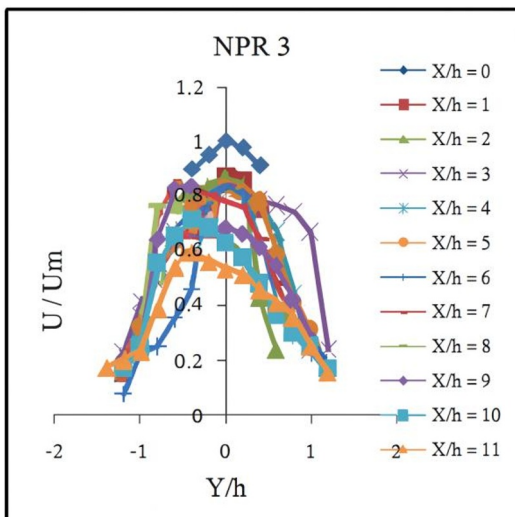


Fig. 6 a

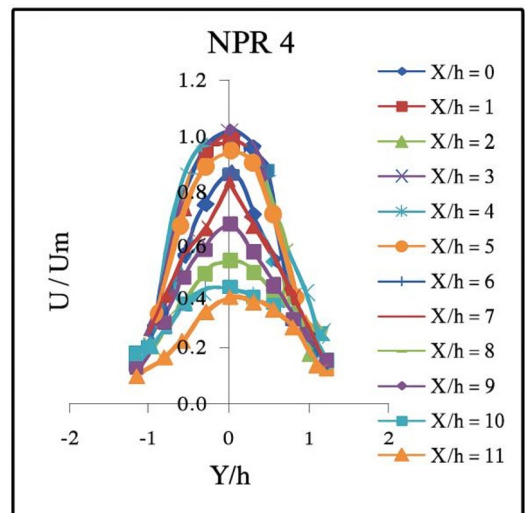


Fig. 6 b

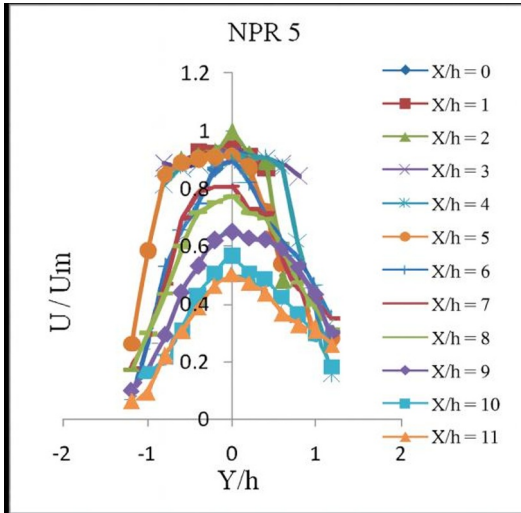


Fig. 6 c

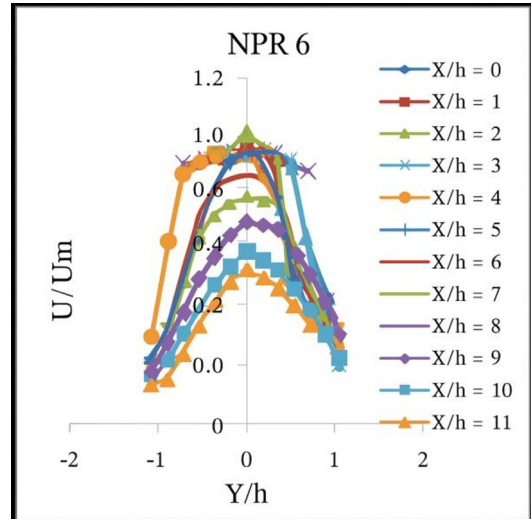


Fig. 6 d

Fig. 6 Variation of non-dimensional velocity (U/U_m) along the transverse direction (Y/h) at different downstream locations (X/h) for (a) NPR 3, (b) NPR 4, (c) NPR 5, and (d) NPR 6.

Figures 3(a-d) show the non-dimensional velocity distribution (U/U_m) in the transverse direction (Y/h) for NPR values 3-6 at various downstream sites. For all NPRs, the velocity peaks at the jet centerline and gradually falls as X/h increases, showing jet core degradation. Higher NPRs (NPRs 5 and 6) retain bigger centerline velocities over longer distances, indicating stronger jet momentum and less early mixing. Throughout the measurement domain, the jet has symmetric velocity profiles about the centreline, showing that the SERN arrangement allows for steady flow development. Jet spreading rises with downstream distance, with NPR 3 having the most lateral development due to a weaker jet core and improved entrainment.

In comparison, NPR 6 has a more limited near-field profile, which is consistent with higher exit pressure and slower mixing. Overall, rising NPR leads to a more collimated jet, slower velocity decay, and less early spreading, whereas lower NPRs favour quicker mixing and wider velocity profiles. These findings demonstrate the sensitivity of SERN jet behaviour to pressure ratio and its impact on mixing and plume shape.

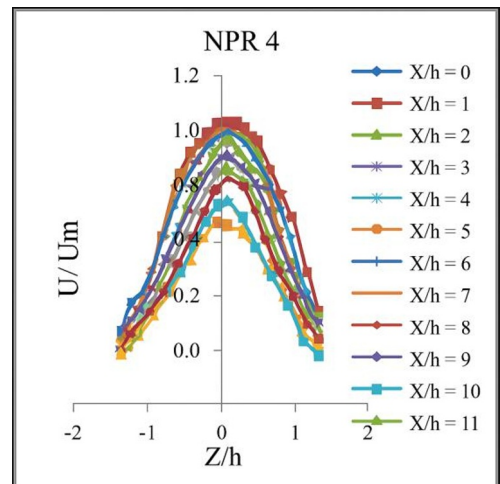
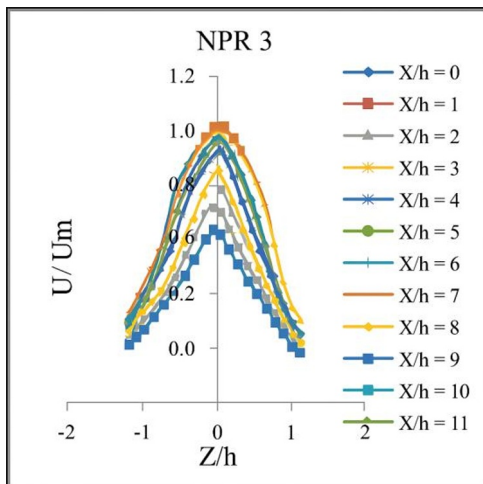


Fig. 7 a

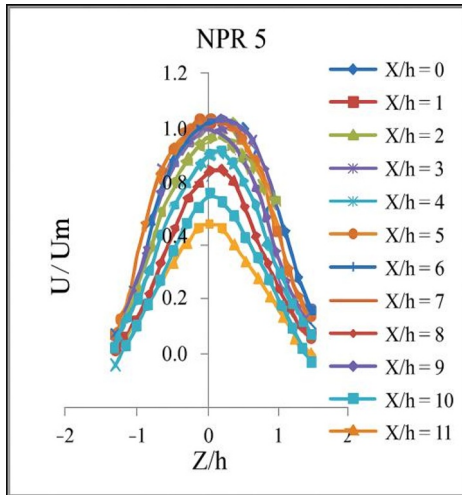


Fig. 7 c

Fig. 7 b

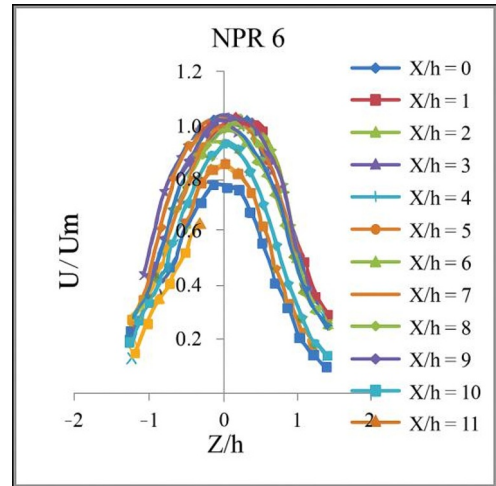


Fig. 7 d

Fig. 7 Variation of non-dimensional velocity (U/U_m) along the transverse direction (Z/h) at different downstream locations (X/h) for (a) NPR 3, (b) NPR 4, (c) NPR 5, and (d) NPR 6.

Figures 7(a-d) depict the non-dimensional velocity distribution (U/U_m) in the vertical direction (Z/h) for NPR values 3, 4, 5, and 6 at various downstream points ($X/h=0$ to 11). All NPRs have a maximum velocity near the jet centre ($Z/h=0$), with peak values ranging from 1.0 to 1.2, and then drop toward the jet edges. This verifies the typical jet-like shape with a high momentum concentration around the centreline. As X/h grows, the peak velocity for each NPR steadily drops, suggesting that the jet decays due to ambient air entrainment.

The degradation is fastest near NPR 3, indicating a weaker jet core and more mixing. In contrast, NPRs 5 and 6 sustain greater centreline velocities across longer downstream lengths, illustrating the stabilizing impact of higher pressure ratios. The dispersion of velocity profiles along Z/h rises downstream for all NPRs, indicating a natural expansion of the jet plume. Lower NPRs have wider and more diffuse profiles, whereas higher NPRs have a more concentrated distribution in the near field. This shows that increasing exit pressure results in a more collimated jet with less early mixing. All NPRs exhibit symmetry about the centreline, showing that the SERN design provides consistent vertical flow characteristics while avoiding considerable asymmetry. Minor differences at large X/h locations are related to increased turbulence and lateral entrainment. Overall, higher NPR results in a stronger jet core, less spreading in the near-field area, and delayed mixing, whereas lower NPRs favour quicker decay and wider plume formation.

4 Conclusion

The work carefully evaluated the non-dimensional velocity distribution of a SERN jet throughout a range of Nozzle Pressure Ratios (NPRs) from 3 to 6, offering key insights into flow dynamics, mixing features, and plume formation. The results repeatedly showed that SERN jet behaviour is very sensitive to the pressure ratio, which controls the strength of the jet core and the rate of mixing with the ambient air. The analysis of the velocity profiles in both the transverse (Y/h) and vertical (Z/h) directions confirmed that higher NPRs, particularly NPRs 5 and 6, retained significantly greater centreline velocities over longer downstream distances, demonstrating the stabilizing impact of higher pressures, which result in a stronger jet momentum and a more robust jet core, delaying decay. Lower NPRs (NPR 3 and 4) had the fastest velocity decrease, indicating a weaker initial jet core and increased mixing.

Furthermore, jet spreading and entrainment were found to be inversely proportional to the NPR: lower NPR 3 showed the most significant lateral and vertical expansion throughout the measurement domain, favouring faster mixing and wider, more diffuse velocity profiles, whereas NPR 6 resulted in a more collimated jet with a confined near-field profile. The continuous symmetry of velocity profiles about the jet centreline in both planes was a key discovery across all tested NPRs, demonstrating that the SERN configuration efficiently allows for stable, predictable flow development without generating considerable asymmetry. Increasing the NPR causes the jet plume to become more concentrated, stronger, more durable, with delayed decay and less near-field spreading. In contrast, decreasing the NPR allows for faster mixing and a larger plume formation. These findings highlight the pressure ratio's direct influence on thrust performance and noise suppression features, confirming that the NPR is a key control parameter for altering the SERN jet's mixing efficiency and overall plume shape.

References

1. G. P. Sutton, *Rocket Propulsion Elements*. New York, NY, USA: John Wiley & Sons, 2001.
2. Yangyu, J. Xu, J. Mo, and M. Wang, "Principal parameters in flow separation patterns of over-expanded single expansion ramp nozzles," *Eng. Appl. Comput. Fluid Mech.*, vol. 8, no. 2, pp. 274–288, 2014, [doi: 10.1080/19942060.2014.11015522](https://doi.org/10.1080/19942060.2014.11015522).
3. K. A. Deere and S. C. Asbury, *Experimental and Computational Investigation of a Translating-Throat, Single-Expansion-Ramp Nozzle*, NASA TP-1999-209138, 1999.
4. V. Thiagarajan, S. Panneerselvam, and E. Rathakrishnan, "Numerical flow visualization of a single expansion ramp nozzle with hypersonic external flow," *Journal of Visualization.*, vol. 9, pp. 91–99, 2006, [doi: 10.1007/BF03181555](https://doi.org/10.1007/BF03181555).
5. E. Besnard, H. H. Chen, and T. Mueller, "Design, manufacturing and test of a plug nozzle rocket engine," in *Proc. AIAA*, Paper 2002-4038, 2002 <https://doi.org/10.2514/6.2002-4038>.
6. W. Huang, Z.-G. Wang, D. B. Ingham, L. Ma, and M. Pourkashanian, "Design exploration for a single expansion ramp nozzle (SERN) using data mining," *Acta Astronaut.*, vol. 83, pp. 10–17, 2013, [doi: 10.1016/j.actaastro.2012.10.028](https://doi.org/10.1016/j.actaastro.2012.10.028).
7. E. Gamble, D. Terrell, and R. De Francesco, "Nozzle selection and design criteria," in *Proc. AIAA*, Paper 2004-3923, 2004 <https://doi.org/10.2514/6.2004-3923>
8. H. Ogawa and R. R. Boyce, "Physical insight into nozzle flow behaviour of axisymmetric scramjets for access-to-space via design optimisation," .
9. S. A. E. Miller and J. Veltin, "Experimental and numerical investigation of flow properties of supersonic helium-air jets," *AIAA Paper* <https://doi.org/10.2514/1.J050720>.
10. F. P. Povinelli and L. A. Povinelli, "Correlation of secondary sonic and supersonic gaseous jet penetration into supersonic crossflows," NASA Report, 1971.
11. S. Raghunath, D. J. Mee, T. Roesgen, and P. A. Jacobs, "Visualization of supersonic flows in shock tunnels using the background-oriented schlieren technique," in *Proc. 10th AIAA Australian Aerospace Student Conf.*, Sydney, Australia, Dec. 2004.
12. G. Yuan, C. Kai, W. Xiuping, H. Shouchao, Y. Guowei, and R. Liang, "Aerodynamic optimization and evaluation for the three-dimensional afterbody/nozzle integrated configuration of hypersonic vehicles," *Sci. China Technol. Sci.*, vol. 57, pp. 849–857, 2012, [doi: 10.1007/s11431-012-4771-y](https://doi.org/10.1007/s11431-012-4771-y).
13. Y. Yu, T. Yu, Y. Mao, Y. Yang, and S. Liang, "Key factors affecting overexpanded flow separation in design of large expansion-ratio single expansion ramp nozzle," *Aeronautical Journal.*, vol. 129, no. 1333, pp. 717–736, 2025, [doi: 10.1017/aer.2024.70](https://doi.org/10.1017/aer.2024.70).

14. Z. Wang, J. Cui, Y. Yang, and Y. Yu, "Simulation and analysis of the over-expanded flow field in asymmetric nozzles with lateral expansion," *International Journal of Turbo & Jet-Engines*, vol. 42, no. 3, pp. 469–481, 2024, [doi: 10.1515/tjj-2024-0033](https://doi.org/10.1515/tjj-2024-0033).
15. S. Vaisakh and T. M. Muruganandam, "Visualization of over-expanded supersonic wall-jet," *Aerospace Science and Technology*, vol. 112, 2021, [doi: 10.1016/J.AST.2021.106617](https://doi.org/10.1016/J.AST.2021.106617).
16. M. Nidharia, "Effect of ramp geometry on single expansion ramp nozzle performance characteristics," *Journal of Propulsion and Power*, vol. 41, no. 1, pp. 1–?, 2025, [doi: 10.2514/1.B39291](https://doi.org/10.2514/1.B39291).
17. K. Whitaker, N. Gowadia, and S. Fordyce, "Thrust vectoring using non-axisymmetric nozzles with flexible contours," *AIAA Paper*, 27th Joint Propulsion Conference, 24–26 June 1991 (or 17 Aug 1991 Online), AIAA-1991-2368, [doi: 10.2514/6.1991-2368](https://doi.org/10.2514/6.1991-2368).
18. K. Xie, X. Chen, J. Li, and Y. Liu, "Introduction," in *Fluidic Nozzle Throats in Solid Rocket Motors*, Singapore: Springer, pp. 1–19, 2019, [doi: 10.1007/978-981-13-6439-6_1](https://doi.org/10.1007/978-981-13-6439-6_1).
19. K. A. Deere and S. C. Asbury, "An experimental and computational investigation of a translating-throat single-expansion-ramp nozzle," *32nd AIAA/ASME/SAE/ASEE Joint Propulsion Conference & Exhibit*, Lake Buena Vista, Florida, 1–3 July 1996, AIAA-96-2540, NASA/TM-111455, 1996, [doi:10.2514/6.1996-2540](https://doi.org/10.2514/6.1996-2540).
20. X. B. Song and Q. Wang, "Design and simulation of the single expansion ramp nozzle (SERN)," *Advanced Materials Research*, vol. 663, pp. 596–601, 2013, [doi: 10.4028/www.scientific.net/AMR.663.596](https://doi.org/10.4028/www.scientific.net/AMR.663.596).